

# A Network-Guided Penalized Regression with Application to Proteomics Data

Seungjun Ahn<sup>1,2</sup> and Eun Jeong Oh<sup>3</sup>

<sup>1</sup>Department of Population Health Science and Policy, Icahn School of Medicine at Mount Sinai, New York, NY 10029, USA

<sup>2</sup>Tisch Cancer Institute, Icahn School of Medicine at Mount Sinai, New York, NY 10029, USA

<sup>3</sup>Institute of Health System Science, Feinstein Institutes for Medical Research, Manhasset, NY 11030, USA

## Abstract

Network theory has proven invaluable in unraveling complex protein interactions. Previous studies have employed statistical methods rooted in network theory, including the Gaussian graphical model, to infer networks among proteins, identifying hub proteins based on key structural properties of networks such as degree centrality. However, there has been limited research examining a prognostic role of hub proteins on outcomes, while adjusting for clinical covariates in the context of high-dimensional data. To address this gap, we propose a network-guided penalized regression method. First, we construct a network using the Gaussian graphical model to identify hub proteins. Next, we preserve these identified hub proteins along with clinically relevant factors, while applying adaptive Lasso to non-hub proteins for variable selection. Our network-guided estimators are shown to have variable selection consistency and asymptotic normality. Simulation results suggest that our method produces better results compared to existing methods and demonstrates promise for advancing biomarker identification in proteomics research. Lastly, we apply our method to the Clinical Proteomic Tumor Analysis Consortium (CPTAC) data and identified hub proteins that may serve as prognostic biomarkers for various diseases, including rare genetic disorders and immune checkpoint for cancer immunotherapy.

**Key words:** Network analysis; Partial penalization; Adaptive Lasso; Proteomics data; Protein interactions; Gaussian graphical model; Network connectivity; CPTAC.

## 1 Introduction

Proteins are key components of human cells and are involved in a diverse range of biological functions such as cell division and metabolism. Proteomics is the study of proteins on a large scale (i.e., proteome) and their interactions in a cell (Pandey & Mann, 2000). Recent advances in mass spectrometry (MS) technology has enabled simultaneous quantification of multiple protein expressions and identification of protein modification

sites for proteomics research (Han et al., 2008; Rozanova et al., 2021). The MS-based proteomics has been increasingly analyzed for biomarker discovery and disease monitoring in complex human diseases such as cancer (Petralia et al., 2024; Wisniewski et al., 2015; Yang et al., 2012), multiple sclerosis (Åkesson et al., 2023), Alzheimer’s disease (Johnson et al., 2022), and alcohol-related liver diseases (Niu et al., 2022). More importantly, a proliferating number of proteomics studies has spurred development of statistical and bioinformatics methods to analyze the proteomics data. The majority of proteins do not act as independent entities. Instead, they work in concert (i.e., protein interactions) to induce and stabilize a range of cellular and physiological responses that include DNA replication, RNA transcription, protein translation, post-translational modification, targeted degradation, signal transduction, and cell cycle control (Manfredi et al., 2019).

The applications of network theory have proven instrumental in inferring the complex landscape of protein interactions through either correlation-based approaches or probabilistic graphical models, similar to other types of -omics disciplines (Shutta et al., 2022). Protein interactions can be represented as large interaction networks, wherein nodes symbolize proteins and edges denote pairwise interactions (co-expression), highlighting the presence of hub nodes based on network properties (e.g. proteins with higher degree centrality) (Vella et al., 2017). Hub proteins play a pivotal role in maintaining the overall structure of a network. Thus, the removal of hub proteins may lead to a severe deterioration of network connectivity than that of non-hub proteins which has been referred to as centrality-lethality rule (Barabási & Oltvai, 2004; He & Zhang, 2006; Jeong et al., 2001). Furthermore, hub proteins are more likely to be encoded by genes associated with diseases than non-hub proteins (Crua Asensio et al., 2017).

Several authors have proposed various methods to estimate protein interactions, either through graphical model estimation or the Weighted Correlation Network Analysis (WGCNA) (Langfelder & Horvath, 2008). Among them, Friedman et al. (2008) introduced the graphical Lasso to estimate sparse undirected networks, which was subsequently validated using a small proteomics dataset. In related work, Lung Cancer Cohort Consortium (LC3) (2023) performed a graphical Lasso-based network analysis on 36 protein biomarkers for imminent lung cancer diagnosis, demonstrating that the structural arrangement of a network changes according to the disease state (case or matched control) and identifying U-PAR as the central hub protein. On the other hand, Johnson et al. (2020) used the WGCNA to identify hub proteins, CD44 and PRDX1, within clusters of densely connected proteins (i.e., modules) which may serve as therapeutic targets for Alzheimer’s disease. Recently, Short et al. (2023) fitted linear regressions to correlate continuous brain MRI outcomes and hub proteins identified from the WGCNA (“eigenproteins” as described in the original paper) while accounting for additional clinical covariates such as age, sex, total/HDL cholesterol ratio, and prevalent cardiovascular diseases.

However, the aforementioned studies have at least two of the following limitations: (1) identified hubs were not adjusted for clinical and demographic covariates; (2) the findings are primarily descriptive, and the investigation into the association between hubs and patient health outcomes remains unexplored, thereby limiting the interpretative framework of the study; and (3) a variable selection was not considered, resulting in a suboptimal prediction model characterized by an increased rate of false positives and reduced statistical power. Especially regarding the third limitation, a pertinent consideration arises – how should we address the retention of specific proteins variables and clinical covariates that may possess significant clinical and biological relevance, irrespective of their prior identification as hallmark biomarkers or genetic factors in

existing studies? This brings into question the rationale for our “*network-guided penalized regression*.”

Another major challenge in proteomics studies is the high-dimensionality of the covariate space. Recent developments in high-dimensional variable selection approaches include penalized regression methods, such as least absolute shrinkage and selection operator (Lasso) (Tibshirani, 1996), adaptive Lasso (Zou, 2006), smoothly clipped absolute deviation method (Fan & Li, 2001), elastic net (Zou & Hastie, 2005), nonnegative garrote (Yuan & Lin, 2007), and many others. Recent studies (Villanueva et al., 2024; Xu et al., 2024) have regressed all proteins in the same prediction model and derived a model with a reduced number of proteins using penalization techniques, including Lasso and elastic net. However, this approach does not consider that a set of proteins interacts with each other as a network. Furthermore, penalizing all proteins is not appropriate when certain variables, such as hubs proteins (for preserving the overall network structure) and clinical covariates (for their clinical importance and potential confounding), should remain in the model. Another study by Tutz and Ulbricht (2009) proposed utilizing the correlation between predictors explicitly in the penalty term. However, their method relies on marginal correlations, which may fail to capture the conditional dependencies among variables that underlie network structures. In contrast, our approach uses partial correlations to reflect direct associations while adjusting for the effects of other protein variables, providing a more biologically meaningful representation of molecular networks.

In the present work, we propose to incorporate network knowledge into variable selection with adaptive Lasso. Specifically, our proposed network-guided penalization procedure retains hub proteins and clinical covariates, while applying an adaptive Lasso penalty to non-hub proteins. The overarching objective of this study is to introduce a method that differentiates hubs from non-hubs and is designed to assess the covariate-adjusted effect of hubs on patient health outcomes with the removal of irrelevant non-hubs. This dual strategy will help preserve the overall network structure by retaining hubs and also enhance the model predictive accuracy by properly adjusting for clinical confounders and penalizing non-hubs for variable selection.

This article is organized into five main sections. Section 1 provides background and motivations. Section 2 covers network estimation, network-guided penalization, and the asymptotic behaviors of the proposed estimators. In Section 3, we present performance metrics from simulation experiments, comparing our method with existing alternatives. In Section 4, we apply our proposed method to proteomics data from the National Cancer Institute (NCI) Clinical Proteomic Tumor Analysis Consortium (CPTAC). Finally, we wrap up our discussion by addressing challenges, limitations, and future directions in Section 5.

## 2 Methods

Consider a finite population of  $n$  subjects. Let  $Y$  be an outcome of interest,  $\mathbf{X} = \{X_1, \dots, X_p\}$  be a vector of proteins,  $\mathbf{Z} = \{Z_1, \dots, Z_c\}$  be a vector of potential confounders that need to be adjusted in the regression, such as age, gender, and other related diseases and conditions at baseline. In our data example,  $\mathbf{X}$  is high-dimensional, whereas the dimension of  $\mathbf{Z}$  is low or moderate.

### 2.1 Network Estimation With Sparse Gaussian Graphical Model

Our idea is built upon the Gaussian graphical model (GGM) (Lauritzen, 1996) to estimate a PPI network, where an edge represents conditional dependency of a pair of nodes (proteins) after controlling for all other nodes in a network. In a GGM network, the weight of an edge is the partial correlation and represent whether

or not and how strongly the two nodes co-occur. Thus, the network structure is decided by an estimation of partial correlations.

We assume  $\mathbf{X}$  follows a multivariate normal distribution:

$$\mathbf{X} \sim N_p(\boldsymbol{\mu}, \boldsymbol{\Sigma}),$$

where  $\boldsymbol{\mu} = (\mu_1, \dots, \mu_p)$  is a vector of means for each protein and  $\boldsymbol{\Sigma} = [\Sigma_{jk}]_{1 \leq j, k \leq p}$  is a  $p \times p$  variance-covariance matrix that is positive definite. The inverse of  $\boldsymbol{\Sigma}$  is a precision matrix (or concentration matrix), denoted by  $\boldsymbol{\Sigma}^{-1} = \boldsymbol{\Theta} = [\theta_{jk}]_{1 \leq j, k \leq p}$ . The off-diagonal elements of precision matrix can be standardized with a sign reversal to calculate the partial correlation of two proteins  $X_j$  and  $X_k$ , conditional on all other proteins in  $\mathbf{X}$  (Shutta et al., 2022), which is our focus in this section,

$$\rho_{X_j, X_k | \mathbf{X}_{-j, -k}} = \frac{-\theta_{jk}}{\sqrt{\theta_{jj}\theta_{kk}}}, \quad (2.1)$$

where  $\mathbf{X}_{-j, -k}$  is a set of proteins without  $j$  and  $k$ , and  $\theta_{jk}$  denotes the corresponding element of  $\boldsymbol{\Theta}$ . Furthermore,  $\boldsymbol{\Theta}$  can be constructed as a network with protein nodes that are connected by edges when  $\rho_{X_j, X_k | \mathbf{X}_{-j, -k}} \neq 0$ .

As in most “-omics” disciplines, there are generally hundreds of samples, while each sample has thousands of proteins (Wang et al., 2021). In the high-dimensional setting where  $n \ll p$ , a maximum likelihood estimation of  $\boldsymbol{\Sigma}$  may not be accurate due to singularity (i.e.,  $\det(\boldsymbol{\Sigma}) = 0$ ) (Kuismin & Sillanpää, 2017). Thereby, a range of regularization methods have been proposed to estimate a sparse GGM, which bypass the issue of  $n \ll p$  and non-invertible  $\boldsymbol{\Sigma}$  (Friedman et al., 2008; Meinshausen & Bühlmann, 2006; Peng et al., 2009).

In the present paper, we consider the graphical Lasso (GL) (Friedman et al., 2008) to impose a sparsity on GGM by penalizing  $\ell_1$ -norm of the elements of  $\boldsymbol{\Theta}$ . The GL estimates  $\boldsymbol{\Theta}$  by maximizing the following penalized log-likelihood:

$$\hat{\boldsymbol{\Theta}} = \underset{\boldsymbol{\Theta}}{\operatorname{argmax}} \{ \log \det(\boldsymbol{\Theta}) - \operatorname{tr}(\hat{\boldsymbol{\Sigma}}\boldsymbol{\Theta}) - \lambda \|\boldsymbol{\Theta}\|_1 \}, \quad (2.2)$$

where  $\hat{\boldsymbol{\Sigma}}$  is an empirical variance-covariance matrix,  $\|\boldsymbol{\Theta}\|_1 = \sum_{j \neq k} |\theta_{j,k}|$  denotes the sum of absolute value of edges, and  $\lambda$  denotes a tuning parameter. The optimal  $\lambda$  can be chosen based on the extended Bayesian information criterion (eBIC) (Foygel & Drton, 2010). The eBIC is expressed as

$$\text{eBIC} = -2\ell(\boldsymbol{\Theta}) + E \log(n) + 4\gamma E \log(p),$$

where  $\ell(\boldsymbol{\Theta})$  is a penalized log-likelihood to estimate  $\hat{\boldsymbol{\Theta}}$  in equation (2.2),  $E$  is a number of edges or non-zero elements of  $\boldsymbol{\Theta}$ , and  $\gamma \in [0, 1]$  denotes a non-negative eBIC hyperparameter. Of note, the eBIC becomes an ordinary BIC when  $\gamma = 0$  and a higher value of  $\gamma$  leads to a greater sparseness by removing more edges (Shutta et al., 2022). Following equation (2.1),  $\hat{\rho}_{jk}$ 's are calculated based on the elements of resulted  $\hat{\boldsymbol{\Theta}}$ . See Figure 1 for an example of the network constructed as described.

The network centrality has been studied to measure the extent of biological or topological importance that

a node has in a network (Ashtiani et al., 2018; Junker & Schreiber, 2008). For each protein  $k$ , the network centrality (degree centrality in continuous scale;  $\hat{\phi}_k$ ) is calculated as the marginal sum of the association matrix.

$$\hat{\phi}_k = \sum_{j=1}^p |\hat{\rho}_{jk}|,$$

where  $k = 1, \dots, p$ . We define protein nodes with higher  $\hat{\phi}_k$  relative to others as hub proteins, where the number of hub proteins  $h < p$  depends on user-specified parameters,  $\delta$  and  $\tau$ , by taking  $h = \min(\lfloor p\delta \rfloor, \tau)$ . More details are discussed in the following subsection.

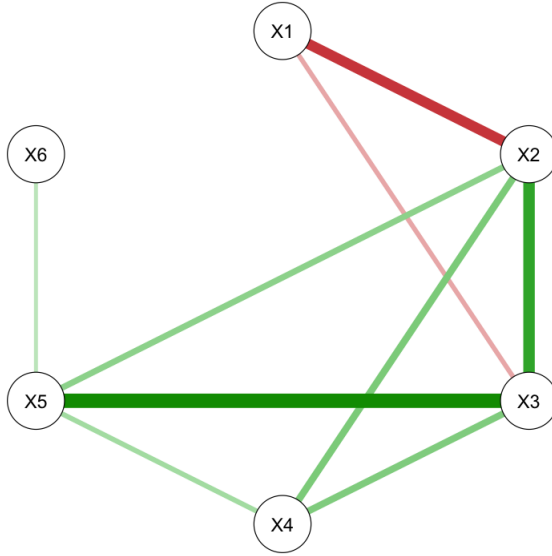


Figure 1: An example network plot to visualize a network with  $p = 6$  proteins based on partial correlation estimates from a graphical Lasso algorithm in combination with an extended Bayesian information criterion. Any missing edge between nodes (e.g.  $X_1 - X_4$ ,  $X_1 - X_5$ , and  $X_1 - X_6$ ) corresponds to a partial correlation estimates of exactly zero in  $\hat{\Theta}$ .

## 2.2 Network-Guided $\ell_1$ -Penalization

Suppose we observe data from  $n$  individuals. For each individual, the data is of the form  $\{\mathbf{Z}, \mathbf{X}, Y\}$ . When the goal is to regress  $\mathbf{Z}, \mathbf{X}$  on  $Y$ , the following model is usually considered:

$$Y = \mu + \mathbf{Z}\boldsymbol{\zeta} + \mathbf{X}\boldsymbol{\eta} + \epsilon, \quad (2.3)$$

where  $\mu$  is the intercept,  $\boldsymbol{\zeta}$  and  $\boldsymbol{\eta}$  are the coefficients for  $\mathbf{Z}$  and  $\mathbf{X}$ , respectively, and  $\epsilon$  is the error component assumed to be normally distributed around zero with constant variance  $\sigma^2$ .

In this project, we decompose  $\mathbf{X}$  into two parts: hub proteins, denoted by  $\mathbf{H} \in \mathbb{R}^h$ , and non-hub proteins, denoted by  $\mathbf{N} = \mathbf{X} \setminus \mathbf{H} \in \mathbb{R}^q$ , such that  $\boldsymbol{\eta} = (\boldsymbol{\eta}_1, \boldsymbol{\eta}_2)$ , where  $\boldsymbol{\eta}_1$  and  $\boldsymbol{\eta}_2$  are the coefficients of  $\mathbf{H}$  and  $\mathbf{N}$ ,

respectively. The network-guided  $\ell_1$ -penalization procedure aims to adjust the level of penalization on non-hub proteins  $\mathbf{N} \in \mathbb{R}^q$ , while preserving hub proteins and potential confounders along with unpenalized intercept, denoted by  $\mathbf{U} = (1, \mathbf{Z}, \mathbf{H}) \in \mathbb{R}^t$ , where  $t = h + c + 1$ , in the model to be adjusted for. Thus, model (2.3) can be re-written as

$$\begin{aligned} Y &= \mu + \mathbf{Z}\boldsymbol{\zeta} + (\mathbf{H}, \mathbf{N})(\boldsymbol{\eta}_1, \boldsymbol{\eta}_2)^\top + \epsilon \\ &= (1, \mathbf{Z}, \mathbf{H})(\mu, \boldsymbol{\zeta}, \boldsymbol{\eta}_1)^\top + \mathbf{N}\boldsymbol{\eta}_2 + \epsilon \\ &= \mathbf{U}\boldsymbol{\alpha} + \mathbf{N}\boldsymbol{\beta} + \epsilon, \end{aligned} \tag{2.4}$$

where  $\boldsymbol{\alpha} = (\mu, \boldsymbol{\zeta}, \boldsymbol{\eta}_1)$  and  $\boldsymbol{\beta} = \boldsymbol{\eta}_2$  are the corresponding coefficients for  $\mathbf{U}$  and  $\mathbf{N}$ , respectively.

To deal with high-dimensional data, we propose a regression approach with a Lasso-type penalty. The network-guided  $\ell_1$ -penalization estimates  $(\hat{\boldsymbol{\alpha}}_n, \hat{\boldsymbol{\beta}}_n)$  are obtained by minimizing the following objective function:

$$L_n(\boldsymbol{\alpha}, \boldsymbol{\beta}) = \|Y - \mathbf{U}\boldsymbol{\alpha} - \mathbf{N}\boldsymbol{\beta}\|_2^2 + \lambda_n \sum_{j=1}^q w_j |\beta_j|,$$

where  $\lambda_n$  is a non-negative tuning parameter that controls model complexity and  $w_j \geq 0$  is the weight for adjusting the level of penalization on  $\beta_j$ . In this project, we apply adaptive Lasso (Zou, 2006) to shrink coefficients of non-hub proteins such that only significant ones remain in the model, while keeping hub proteins and clinical covariates. In adaptive Lasso, the weight vector is defined as  $\hat{\mathbf{w}} = |\tilde{\boldsymbol{\beta}}_n|^{-\nu}$  for some  $\nu > 0$ , where  $\tilde{\boldsymbol{\beta}}_n$  is any root- $n$ -consistent estimator. This imposes heavier penalties on covariates with smaller coefficients. In practice, we use perturbed elastic net estimates for  $\tilde{\boldsymbol{\beta}}_n$ , following Zou and Zhang (2009). The 5- or 10-fold cross-validation can be used to select an optimal pair of  $(\nu, \lambda_n)$ .

The formula  $h = \min(\lfloor p\delta \rfloor, \tau)$  which is used to identify  $\mathbf{H}$  helps control that the number of hub proteins depends on a user-specified proportion to the size of  $\mathbf{X}$  with the pre-specified positive constant  $\tau$ . In this study, we set  $\tau = \lfloor (p + 20)/16 \rfloor$ , such that the dimension of non-penalized terms is moderate. It is essential that starting with the minimal size of  $\mathbf{H}$  is desired due to the nature of a partial penalization. Even if all essential proteins were not classified as  $\mathbf{H}$ , they would still undergo evaluation as  $\mathbf{N}$  through a penalization method and could remain in the final model if they are shown to be predictive of outcomes in a data-driven manner.

We assume the following two regularity conditions:

(A1)  $\epsilon \triangleq Y - \mathbf{U}\boldsymbol{\alpha}_0 - \mathbf{N}\boldsymbol{\beta}_0$  has mean zero and finite variance  $\sigma^2$ , and is independent of  $(\mathbf{U}, \mathbf{N})$ .

(A2)  $n^{-1}(\mathbf{U}, \mathbf{N})^\top (\mathbf{U}, \mathbf{N}) \rightarrow \mathbf{C}$ , where  $\mathbf{C}$  is positive definite.

Let  $\mathcal{J} = \{j : \beta_{0j} \neq 0, j = 1, \dots, q\}$  be the true active set of variables in  $\mathbf{N}$ , and assume that  $|\mathcal{J}| = r < q$ . Denote the estimated active set of variables by  $\hat{\mathcal{J}}_n = \{j : \hat{\beta}_{nj} \neq 0, j = 1, \dots, q\}$ . Let  $\boldsymbol{\beta}_{0\mathcal{J}} = \{\beta_{0j} : j \in \mathcal{J}\}$  and  $\hat{\boldsymbol{\beta}}_{n\mathcal{J}} = \{\hat{\beta}_{nj} : j \in \mathcal{J}\}$ . Denote  $\boldsymbol{\theta} = (\boldsymbol{\alpha}^\top, \boldsymbol{\beta}^\top)^\top$  for any  $\boldsymbol{\alpha} \in \mathbb{R}^t$ ,  $\boldsymbol{\beta} \in \mathbb{R}^q$ . Then  $\mathcal{S} = \{1, 2, \dots, t\} \cup \{s : \theta_{0s} \neq 0, s = t + 1, \dots, t + q\}$  is the true active set of variables in  $(\mathbf{U}, \mathbf{N})$ , and thus  $\mathcal{J}$  is always the subset of  $\mathcal{S}$ . Denote  $\mathbf{C}_{\mathcal{S}} \in \mathbb{R}^{(t+r) \times (t+r)}$  is the top-left block matrix (i.e., sub-matrix) of  $\mathbf{C} \in \mathbb{R}^{(t+q) \times (t+q)}$ . In the following, we demonstrate the oracle property of our estimators.

**Theorem 1.** Suppose  $\lambda_n = o(\sqrt{n})$  and  $\lambda_n n^{(\nu-1)/2} \rightarrow \infty$ . Then under model (2.4) and regularity conditions (A1)–(A2), the network-guided adaptive Lasso estimators satisfy the following properties:

- i) (variable selection consistency)  $\lim_n P(\hat{\mathcal{J}}_n = \mathcal{J}) = 1$ ,
- ii) (joint asymptotic normality)

$$\sqrt{n} \begin{pmatrix} \hat{\boldsymbol{\alpha}}_n - \boldsymbol{\alpha}_0 \\ \hat{\boldsymbol{\beta}}_{n\mathcal{J}} - \boldsymbol{\beta}_{0\mathcal{J}} \end{pmatrix} \rightarrow_d N(\mathbf{0}, \sigma^2 \mathbf{C}_S^{-1}).$$

The theorem above implies that the network-guided adaptive Lasso estimators enjoys variable selection consistency and asymptotic normality. The proof is deferred to the Appendix.

### 3 Simulation Experiments

In this section, simulation studies are conducted to compare the proposed network-guided (NG) adaptive Lasso estimators with other existing alternatives and evaluate model performance using various metrics. We make a comparison with the adaptive Lasso (aLasso), Lasso, elastic net (enet), and ridge regression models, as well as the correlation-based penalized estimators (CBPE) proposed by Tutz and Ulbricht (2009). For each method, the 5-fold cross-validation was used to select the optimal tuning parameters.

#### 3.1 Settings

We generated  $\mathbf{X}$  from the multivariate normal distribution  $N_p(\mathbf{0}, \boldsymbol{\Sigma})$  with the correlation structure  $\boldsymbol{\Sigma} = [\Sigma_{jk}]_{1 \leq j, k \leq p}$ , where  $\Sigma_{jk}$  is 1 if  $j = k$ , 0.9 if  $j \in \{1, 2, 3, 4\} \neq k$ , and  $0.9^{|j-k|}$  if  $j \in \{5, \dots, p\} \neq k$ . Three potential confounders were generated as follows:  $Z_1 \sim U(0, 1)$ ,  $Z_2 \sim \text{Bernoulli}(0.25)$ , and  $Z_3 \sim \text{Bernoulli}(0.65)$ . The outcome variable was generated according to the model (2.3) with  $\sigma = 1$ ,  $\mu = 0.5$ ,  $\boldsymbol{\zeta} = (2.5, 2.5, 2.5)$  along with the two different scenarios for  $\boldsymbol{\eta}$ :

1. Strong signal:  $\boldsymbol{\eta} = (3.5_5, 0_5, -1.5_5, 0_{p-15})$
2. Weak signal:  $\boldsymbol{\eta} = (1, -0.8, 0.6, 0, 0, -1.5, -0.5, 1.2, 0_{p-8})$

Different combinations of sample size and dimension (network size), denoted as  $(n, p) = (50, 60), (100, 60), (100, 300)$ , were considered. Following the terms used in Monti and Filzmoser (2021), each sample size/dimension combination represents moderate-high-dimensional ( $n < p$ ), low-high-dimensional ( $n > p$ ), and high-dimensional setting ( $n \ll p$ ), respectively. The high-dimensional setting is often observed in proteomics studies, as in most “-omics” disciplines. For each setting, we repeated the simulation 100 times.

#### 3.2 Performance metrics

The predictive model performance is mainly evaluated using the root-mean-squared error (RMSE) and calibration slope (CSL). Overall variable selection performance was assessed by the F1 score, defined as

$$\text{F1 score} = \frac{2 \cdot \text{TP}}{2 \cdot \text{TP} + \text{FP} + \text{FN}},$$

and the Matthews correlation coefficient (MCC) proposed by Matthews (1975), defined as

$$\text{MCC} = \frac{\text{TP} \cdot \text{TN} - \text{FP} \cdot \text{FN}}{\sqrt{(\text{TP} + \text{FP}) \cdot (\text{TP} + \text{FN}) \cdot (\text{TN} + \text{FP}) \cdot (\text{TN} + \text{FN})}},$$

where TP, TN, FP, and FN are true positives, true negatives, false positives, and false negatives, respectively. The performance measures were evaluated on an independent test set of size 1,000.

### 3.3 Simulation results

Tables 1–2 present model performance metrics under various settings based on 100 simulation replicates. For each metric, the mean value is reported along with the standard deviation in parentheses. In the strong signal case (Table 1), with different specifications of  $\delta$ , our proposed NG method consistently outperformed other existing methods, in terms of lower RMSE, better calibration, higher F1 score, and higher MCC. Especially when  $n > p$ , aLasso and our NG method performed well, in terms of calibration slope nearly close to an ideal value of 1 and a very high MCC.

However, it is worth noting that in settings where the number of proteins is greater or significantly greater than the number of observations (i.e.,  $n < p$  or  $n \ll p$ ), our NG method showed much better performances than the alternative methods. For example, when  $n < p$ , the NG method had a F1 score of 0.81, which was higher than the rest of the methods, ranging from 0.34 (ridge or CBPE) to 0.71 (aLasso). Furthermore, the proposed NG method demonstrated a smaller standard deviation of RMSE, compared to the competing methods. When  $n \ll p$ , the RMSE standard deviations were 0.11 (NG,  $\delta = 0.01$ ) and 0.13 (NG,  $\delta = 0.02$  or  $\delta = 0.03$ ), which were smaller than 0.90 (ridge) or 0.46 (aLasso). Additionally, ridge, enet, and CBPE showed poor performance, characterized by one or more of the following: high RMSE, calibration slope far from 1, low F1 score, or low MCC.

Similarly, in the weak signal case (Table 2), our proposed NG method continued to outperform the other methods. For instance, in the high-dimensional setting  $n \ll p$ , the RMSE of the NG method with  $\delta = 0.02$  was 0.19, which was less than half of that of aLasso (RMSE, 0.45), Lasso (RMSE, 0.46), and enet (RMSE, 0.53), and almost one-tenth of ridge (RMSE, 2.14) or CBPE (RMSE, 2.48). In all settings, the NG method showed lower RMSE, better calibration, higher F1 score, and higher MCC.

In all cases, our method consistently performed well even with a small  $\delta$ . As discussed in Section 2.2, proteins that may have been initially missed out based our network estimation can still be included in the final model through variable selection if they show predictive potential, thereby demonstrating good overall model performance.

Table 1: Simulation results under strong signal case using network-guided (NG) method, adaptive Lasso (aLasso), Lasso, elastic net (enet), ridge regression, and correlation-based penalized estimators (CBPE). The best results are highlighted in boldface.

Setting	$n$	$p$	Method	RMSE	CSL	F1 score	MCC
$n < p$	50	60	NG ( $\delta = 0.06$ )	1.33 (0.59)	<b>1.01</b> (0.01)	<b>0.81</b> (0.11)	0.75 (0.15)
			NG ( $\delta = 0.08$ )	<b>1.32</b> (0.57)	<b>1.01</b> (0.01)	<b>0.81</b> (0.11)	<b>0.77</b> (0.14)
			NG ( $\delta = 0.10$ )	<b>1.32</b> (0.63)	<b>1.01</b> (0.01)	<b>0.81</b> (0.10)	0.76 (0.13)
			aLasso	2.89 (0.78)	1.04 (0.03)	0.71 (0.15)	0.66 (0.19)
			Lasso	1.88 (0.71)	1.03 (0.02)	0.64 (0.10)	0.56 (0.14)
			enet	2.22 (0.58)	1.04 (0.02)	0.52 (0.07)	0.40 (0.11)
			ridge	8.16 (0.72)	1.63 (0.14)	0.34 (0.00)	–
			CBPE	2.77 (0.31)	1.04 (0.03)	0.34 (0.00)	–
$n > p$	100	60	NG ( $\delta = 0.06$ )	<b>0.67</b> (0.10)	<b>1.01</b> (0.00)	<b>0.99</b> (0.03)	<b>0.98</b> (0.03)
			NG ( $\delta = 0.08$ )	0.68 (0.11)	<b>1.01</b> (0.00)	0.98 (0.03)	<b>0.98</b> (0.03)
			NG ( $\delta = 0.10$ )	0.70 (0.11)	<b>1.01</b> (0.00)	0.95 (0.03)	0.94 (0.04)
			aLasso	0.70 (0.10)	<b>1.01</b> (0.00)	0.98 (0.04)	<b>0.98</b> (0.04)
			Lasso	0.74 (0.12)	1.02 (0.00)	0.71 (0.07)	0.65 (0.08)
			enet	0.89 (0.14)	1.02 (0.00)	0.51 (0.05)	0.41 (0.07)
			ridge	0.94 (0.11)	1.02 (0.01)	0.34 (0.00)	–
			CBPE	1.57 (0.17)	1.02 (0.01)	0.34 (0.00)	–
$n \ll p$	100	300	NG ( $\delta = 0.01$ )	<b>1.08</b> (0.11)	<b>1.00</b> (0.00)	<b>0.97</b> (0.03)	<b>0.97</b> (0.03)
			NG ( $\delta = 0.02$ )	1.15 (0.13)	<b>1.00</b> (0.00)	0.88 (0.03)	0.87 (0.03)
			NG ( $\delta = 0.03$ )	1.19 (0.13)	<b>1.00</b> (0.00)	0.79 (0.03)	0.78 (0.03)
			aLasso	2.42 (0.46)	1.02 (0.01)	0.85 (0.06)	0.86 (0.05)
			Lasso	1.15 (0.21)	1.02 (0.00)	0.92 (0.06)	0.92 (0.05)
			enet	1.22 (0.23)	1.02 (0.00)	0.85 (0.07)	0.85 (0.07)
			ridge	9.87 (0.90)	1.45 (0.07)	0.08 (0.00)	–
			CBPE	5.29 (0.33)	1.07 (0.02)	0.08 (0.00)	–

Abbreviations: RMSE, root-mean-squared error; CSL, calibration slope  
 $\delta$  is the proportion used for the number of hub protein nodes in a network

Table 2: Simulation results under weak signal case using network-guided (NG) method, adaptive Lasso (aLasso), Lasso, elastic net (enet), ridge regression, and correlation-based penalized estimators (CBPE). The best results are highlighted in boldface.

Setting	$n$	$p$	Method	RMSE	CSL	F1 score	MCC
$n < p$	50	60	NG ( $\delta = 0.06$ )	0.26 (0.10)	<b>1.01</b> (0.02)	<b>0.88</b> (0.08)	<b>0.86</b> (0.09)
			NG ( $\delta = 0.08$ )	0.23 (0.10)	<b>1.01</b> (0.02)	0.87 (0.07)	0.85 (0.08)
			NG ( $\delta = 0.10$ )	<b>0.20</b> (0.08)	<b>1.01</b> (0.01)	0.86 (0.06)	0.83 (0.06)
			aLasso	0.49 (0.11)	1.07 (0.04)	0.80 (0.05)	0.79 (0.06)
			Lasso	0.34 (0.14)	1.05 (0.03)	0.62 (0.09)	0.58 (0.11)
			enet	0.46 (0.14)	1.07 (0.04)	0.53 (0.07)	0.48 (0.09)
			ridge	2.06 (0.11)	3.43 (3.41)	0.25 (0.00)	–
			CBPE	0.89 (0.12)	0.97 (0.04)	0.25 (0.00)	–
$n > p$	100	60	NG ( $\delta = 0.06$ )	<b>0.08</b> (0.01)	1.01 (0.00)	0.96 (0.02)	0.96 (0.03)
			NG ( $\delta = 0.08$ )	<b>0.08</b> (0.01)	<b>1.00</b> (0.00)	0.95 (0.01)	0.94 (0.01)
			NG ( $\delta = 0.10$ )	<b>0.08</b> (0.01)	<b>1.00</b> (0.00)	0.91 (0.02)	0.89 (0.02)
			aLasso	<b>0.08</b> (0.01)	1.01 (0.00)	<b>1.00</b> (0.00)	<b>1.00</b> (0.00)
			Lasso	<b>0.08</b> (0.01)	1.02 (0.00)	0.78 (0.07)	0.77 (0.07)
			enet	0.09 (0.01)	1.02 (0.00)	0.64 (0.07)	0.62 (0.07)
			ridge	0.54 (0.05)	1.10 (0.03)	0.25 (0.00)	–
			CBPE	0.36 (0.04)	0.96 (0.01)	0.25 (0.00)	–
$n \ll p$	100	300	NG ( $\delta = 0.01$ )	0.28 (0.08)	<b>1.01</b> (0.01)	<b>0.87</b> (0.07)	<b>0.87</b> (0.07)
			NG ( $\delta = 0.02$ )	<b>0.19</b> (0.06)	<b>1.01</b> (0.01)	0.81 (0.02)	0.80 (0.03)
			NG ( $\delta = 0.03$ )	0.20 (0.07)	<b>1.01</b> (0.01)	0.70 (0.02)	0.71 (0.03)
			aLasso	0.45 (0.06)	1.05 (0.02)	0.81 (0.03)	0.82 (0.03)
			Lasso	0.46 (0.05)	1.06 (0.02)	0.44 (0.09)	0.47 (0.07)
			enet	0.53 (0.07)	1.08 (0.03)	0.33 (0.06)	0.39 (0.05)
			ridge	2.14 (0.12)	1.83 (0.60)	0.06 (0.00)	–
			CBPE	2.48 (0.22)	0.73 (0.07)	0.06 (0.00)	–

Abbreviations: RMSE, root-mean-squared error; CSL, calibration slope  
 $\delta$  is the proportion used for the number of hub protein nodes in a network

## 4 Real Data Application

### 4.1 Clinical Proteomic Tumor Analysis Consortium Data

A pre-processed MS-based proteomics data of the National Cancer Institute (NCI) Clinical Proteomic Tumor Analysis Consortium (CPTAC) was downloaded from the Proteomic Data Commons (PDC; <https://pdc.cancer.gov/pdc/cptac-pancancer>), which is one of the largest public repositories of proteogenomic data. In this paper, the Estimation of STromal and Immune cells in MAlignant Tumor tissues using Expression data (ESTIMATE) (Yoshihara et al., 2013) score is the outcome of interest. The ESTIMATE score is a sum of the scores of immune and stromal cells, the two main non-tumor components in the tumor microenvironment. It has been used in a variety of cancer studies such as osteosarcoma (Zhang et al., 2020), head-and-neck squamous cell carcinoma (HNSCC) (Liu et al., 2023), and lung cancer (Lehtiö et al., 2021). The higher the score, the lower the purity of the tumor. The clinical covariates that are included in the modeling with proteins are age, sex, body mass index (BMI), cancer staging, and size of tumor.

### 4.2 Analysis

We analyzed 337 gene-level proteins that are subsets of B cell-immune module from 108 patients with HNSCC. B cell-immune module was the rarest that accounts only in 3% of identified modules depicted in a recent study (Petrulia et al., 2024). Of note, B cells have the ability to promote humoral immunity through the production of antibodies and its presence has been associated with responses to immunotherapy in cancer studies (Garaud et al., 2019; Ruffin et al., 2021).

Table 3 summarizes characteristics of the full cohort sample, and we stratified these characteristics by smoking status. The study samples comprised older adults (median [IQR] = 62.0 [11.3]), predominantly male (87%), and normal weights (24.0 [5.9]), according to the Centers for Disease Control and Prevention (Weir & Jan, 2023). 70.4% of patients were found in tumors staged III or IV with the median size of tumor was 3.2 cm (IQR=1.8). The ESTIMATE scores were significantly different across smoking statuses. In general, non-smokers had higher ESTIMATE scores in all cancer stages from early (stage I) to advanced disease (stage IV), when compared with current and past smokers. This is shown as side-by-side box plots in Figure 2.

Further, our proposed method was benchmarked on the CPTAC-HNSCC data against other popular methods that were evaluated in our simulation experiments above. When applying our method, three different values were considered for  $\delta$ , the proportion of hub proteins in a network. We hypothesize that 3 ( $\delta = 0.01$ ), 6 ( $\delta = 0.02$ ), and 10 ( $\delta = 0.03$ ) out of 337 gene-level proteins from B-cell immune module are defined as hubs in a network. As a whole, Table 4 shows that our NG method had lower RMSE and better calibration slope (closer to 1) than that of the benchmark models.

In addition to benchmark results, the HUGO Gene Nomenclature Committee (HGNC)-approved symbols of covariate-adjusted hub proteins are listed in Table 5. HGNC-approved symbols are protein-coding gene annotations for each known human gene (Seal et al., 2023). In this analysis, PABPC1, LGALS1, and GIMAP7 were found in common between three different values for  $\delta$  parameter. By searching through integrative databases of human genes (GeneCards (Stelzer et al., 2016)) and human diseases (MalaCards (Rappaport et al., 2017)), PABPC1 is linked to viral diseases that are transmitted by mosquitoes such as

rift valley fever and dengue virus. LGALS1 is related to corneal ulcer. Interestingly, a recent study (Qin et al., 2022) suggested that GIMAP7 has a potential as a prognostic biomarker and immune checkpoint gene for immunotherapy in pan-cancer. Additional hub proteins were identified when increasing the size of  $\delta$ . BLNK is associated with a rare genetic immunodeficiency disorder, called autosomal agammaglobulinemia (Cardenas-Morales & Hernandez-Trujillo, 2017).

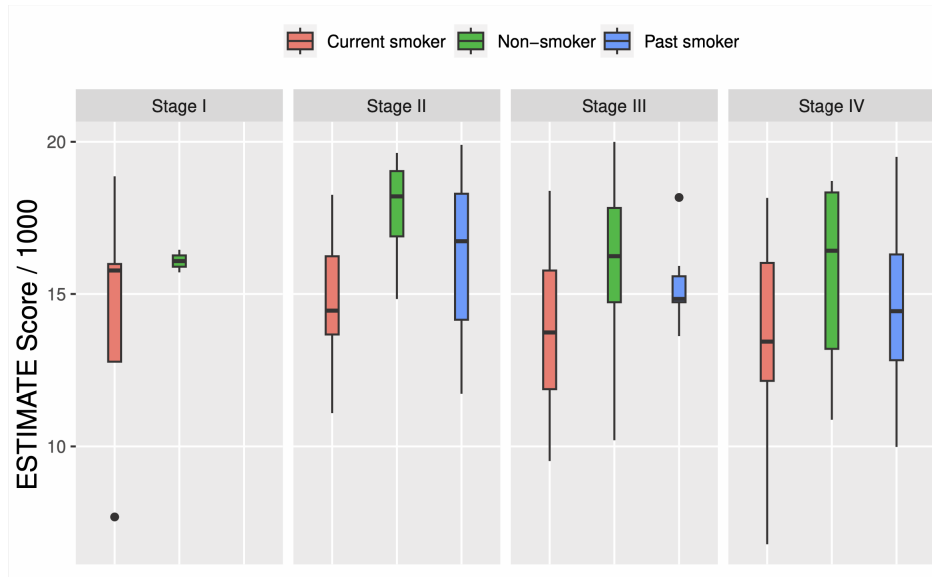


Figure 2: Side-by-side boxplots to visualize the distributions of scaled ESTIMATE scores (scores divided by 1000) of CPTAC-HNSCC patients ( $n = 108$ ) by smoking status and cancer staging.

Table 3: Patient characteristics of CPTAC-HNSCC patients.

Characteristics	Overall N = 108	Current smoker N = 61	Non-smoker N = 20	Past smoker N = 27	p-value <sup>4</sup>
Age in years <sup>1</sup>	62.0 (11.3)	62.0 (12.0)	59.5 (11.3)	64.0 (9.0)	0.2
Sex <sup>2</sup>					0.005
Female	14 (13.0%)	8 (13.1%)	6 (30.0%)	0 (0.0%)	
Male	94 (87.0%)	53 (86.9%)	14 (70.0%)	27 (100.0%)	
BMI <sup>1</sup>	24.0 (5.9)	24.0 (5.2)	24.6 (6.2)	24.0 (5.7)	0.005
Cancer staging <sup>2</sup>					0.7
Stage I	7 (6.5%)	5 (8.2%)	2 (10.0%)	0 (0.0%)	
Stage II	25 (23.1%)	14 (23.0%)	4 (20.0%)	7 (25.9%)	
Stage III	30 (27.8%)	16 (26.2%)	7 (35.0%)	7 (25.9%)	
Stage IV	46 (42.6%)	26 (42.6)	7 (35.0%)	13 (48.1)	
Tumor size in cm <sup>1</sup>	3.2 (1.8)	3.0 (2.0)	3.1 (1.4)	4.0 (1.3)	0.5
ESTIMATE score <sup>3</sup>	14.8 (4.0)	13.9 (3.7)	16.4 (3.5)	15.2 (3.4)	0.005

Abbreviations: BMI, body mass index

Median (IQR)

n(%)

Scaled (score divided by 1000)

Kruskal-Wallis test or Fisher's exact test as appropriate

Table 4: Analyses of CPTAC-HNSCC patients using network-guided (NG) method, adaptive Lasso (aLasso), Lasso, elastic net (enet), ridge regression, and correlation-based penalized estimators (CBPE). The best results are highlighted in boldface.

	RMSE	CSL
NG ( $\delta = 0.01$ )	1.95	<b>0.95</b>
NG ( $\delta = 0.02$ )	1.78	<b>0.95</b>
NG ( $\delta = 0.03$ )	<b>1.77</b>	0.89
aLasso	1.80	1.07
Lasso	2.01	1.88
Ridge	2.27	2.27
enet	1.90	1.51
CBPE	2.94	0.56

Abbreviations: RMSE, root-mean-squared error; CSL, calibration slope

 $\delta$  is the proportion used for the number of hub protein nodes in a networkTable 5: A complete list of significantly connected hub proteins that are adjusted by covariates. Results are shown by varying sizes of the proportion of hub proteins in a network ( $\delta$ ). Listed proteins are mapped to gene symbols approved by the HUGO Gene Nomenclature Committee (HGNC). Proteins that are found in common between all three  $\delta$  are boldfaced.

HGNC Approved Symbols of Covariate-Adjusted Hub Proteins	
NG ( $\delta = 0.01$ )	<b>PABPC1, LGALS1, GIMAP7</b>
NG ( $\delta = 0.02$ )	<b>PABPC1, LGALS1, GIMAP7</b> , MEN1, RPLP1, HNRNPD
NG ( $\delta = 0.03$ )	<b>PABPC1, LGALS1, GIMAP7</b> , MEN1, RPLP1, HNRNPD, CASP10, BLNK, SDC1, MUC4

## 5 Discussion

In this study, we have proposed a network-guided penalized regression model that retains hub proteins and clinical covariates, applying an adaptive Lasso penalty exclusively to non-hub proteins. This model screens out irrelevant non-hub proteins based on their predictive value, while maintaining key variables, including potential confounders for their clinical importance and hub proteins that are identified through network estimation. Our hybrid method leverages network estimation and variable selection through partial penalization, representing a novel approach. We have also shown that our network-guided estimators enjoy variable selection consistency and asymptotic normality.

Through a series of simulation studies and real data application, we have observed that the proposed network-guided approach demonstrates good overall performance measures. It is noteworthy that our method shines particularly in high-dimensional settings, where the number of proteins significantly exceeds the number of observations ( $n \ll p$ ), which is a common scenario in most “-omics” disciplines.

Incorporating hub proteins is crucial, as they may serve as prognostic biomarkers across diverse diseases, including rare genetic disorders and immune checkpoints in cancer immunotherapy. Hub nodes can be identified based on various network properties. Here, we opted for degree centrality due to its intuitive nature and popularity in the literature. Future studies are warranted for the adoption of different network properties, such as betweenness and closeness centrality, to investigate how these impact results. It is also of interest to consider more flexible regression approaches which could handle repeatedly measured proteins data and/or complex relationships (e.g., non-linear or piece-wise) between covariates and the outcome of interest.

## References

- Åkesson, J., Hojjati, S., Hellberg, S., Raffetseder, J., Khademi, M., Rynkowski, R., Kockum, I., Altafini, C., Lubovac-Pilav, Z., Mellergård, J., Jenmalm, M., Piehl, F., Olsson, T., Ernerudh, J., & M, G. (2023). Proteomics reveal biomarkers for diagnosis, disease activity and long-term disability outcomes in multiple sclerosis. *Nat Commun*, *14*(1), 6903.
- Ashtiani, M., Salehzadeh-Yazdi, A., Razaghi-Moghadam, Z., Hennig, H., Wolkenhauer, O., Mirzaie, M., & Jafari, M. (2018). A systematic survey of centrality measures for protein-protein interaction networks. *BMC Syst Biol*, *12*, 80.
- Barabási, A., & Oltvai, Z. (2004). Network biology: Understanding the cell’s functional organization. *Nat Rev Genet*, *5*(2), 101–113.
- Cardenas-Morales, M., & Hernandez-Trujillo, V. (2017). Agammaglobulinemia: from X-linked to Autosomal Forms of Disease. *Clin Rev Allergy Immunol*, *63*(1), 22–35.
- Crua Asensio, N., Muñoz Giner, E., de Groot, N., & Torrent Burgas, M. (2017). Centrality in the host-pathogen interactome is associated with pathogen fitness during infection. *Nat Commun*, *8*, 14092.
- Fan, J., & Li, R. (2001). Variable selection via nonconcave penalized likelihood and its oracle properties. *Journal of the American Statistical Association*, *96*(456), 1348–1360.
- Foygel, R., & Drton, M. (2010). Extended bayesian information criteria for gaussian graphical models. *Advances in neural information processing systems*, *23*, 604–612.

- Friedman, J., Hastie, T., & Tibshirani, R. (2008). Sparse inverse covariance estimation with the graphical lasso. *Biostatistics*, *9*, 432–441.
- Garaud, S., Buisseret, L., Solinas, C., et al. (2019). Tumor infiltrating b-cells signal functional humoral immune responses in breast cancer. *JCI Insight*, *5*(18), e129641.
- Geyer, C. (1994). On the asymptotics of constrained m-estimation. *Annals of Statistics*, *22*, 1993–2010.
- Han, X., Aslanian, A., & Yates III, J. (2008). Mass spectrometry for proteomics. *Curr Opin Chem Biol*, *12*(5), 483–490.
- He, X., & Zhang, J. (2006). Why do hubs tend to be essential in protein networks? *PLoS Genetics*, *2*(6), e88.
- Jeong, H., Mason, S., Barabási, A., & Oltvai, Z. (2001). Lethality and centrality in protein networks. *Nature*, *411*(6833), 41–42.
- Johnson, E., Carter, E., Dammer, E., Duong, D., Gerasimov, E., Liu, Y., et al. (2022). Large-scale deep multi-layer analysis of alzheimer’s disease brain reveals strong proteomic disease-related changes not observed at the rna level. *Nat Neurosci*, *25*(2), 213–225.
- Johnson, E., Dammer, E., Duong, D., Ping, L., Zhou, M., Yin, L., et al. (2020). Large-scale proteomic analysis of alzheimer’s disease brain and cerebrospinal fluid reveals early changes in energy metabolism associated with microglia and astrocyte activation. *Nature Medicine*, *26*(5), 769–780.
- Junker, B., & Schreiber, F. (2008). *Analysis of biological networks*. John Wiley & Sons.
- Knight, K., & Fu, W. (2000). Asymptotics for lasso-type estimators. *Annals of Statistics*, *28*(5), 1356–1378.
- Kuismin, M., & Sillanpää, M. (2017). Estimation of covariance and precision matrix, network structure, and a view toward systems biology. *Wiley Interdisciplinary Reviews: Computational Statistics*, *9*, 1–13.
- Langfelder, P., & Horvath, S. (2008). WGCNA: an R package for weighted correlation network analysis. *BMC bioinformatics*, *9*(559).
- Lauritzen, S. (1996). *Graphical models*. Oxford University Press.
- Lehtiö, J., Arslan, T., Siavelis, I., et al. (2021). Proteogenomics of non-small cell lung cancer reveals molecular subtypes associated with specific therapeutic targets and immune evasion mechanisms. *Nat Cancer*, *2*(11), 1224–1242.
- Liu, Z., Meng, X., Tang, X., Zou, W., & He, Y. (2023). Intratumoral tertiary lymphoid structures promote patient survival and immunotherapy response in head neck squamous cell carcinoma. *Cancer Immunol Immunother*, *72*(6), 1505–1521.
- Lung Cancer Cohort Consortium (LC3). (2023). The blood proteome of imminent lung cancer diagnosis. *Nature Communications*, *14*(1), 3042.
- Manfredi, M., Brandi, J., Di Carlo, C., Vita Vanella, V., Barberis, E., Marengo, E., Patrone, M., & Cecconi, D. (2019). Mining cancer biology through bioinformatic analysis of proteomic data. *Expert Rev Proteomics*, *16*(9), 733–747.
- Matthews, B. W. (1975). Comparison of the predicted and observed secondary structure of t4 phage lysozyme. *Biochimica et Biophysica Acta (BBA)-Protein Structure*, *405*(2), 442–451.
- Meinshausen, N., & Bühlmann, P. (2006). High-dimensional graphs and variable selection with the lasso. *Annals of Statistics*, *34*, 1436–1462.
- Monti, G. S., & Filzmoser, P. (2021). Sparse least trimmed squares regression with compositional covariates for high-dimensional data. *Bioinformatics*, *37*(21), 3805–3814.

- Niu, L., Thiele, M., Geyer, P., Rasmussen, D., Webel, H., Santos, A., et al. (2022). Noninvasive proteomic biomarkers for alcohol-related liver disease. *Nat Med*, *28*(6), 1277–1287.
- Pandey, A., & Mann, M. (2000). Proteomics to study genes and genomes. *Nature*, *405*(6788), 837–846.
- Peng, J., Wang, P., Zhou, N., & Zhu, J. (2009). Partial correlation estimation by joint sparse regression models. *J. Am. Stat. Assoc.*, *104*, 735–746.
- Petralia, F., Ma, W., Yaron, T., et al. (2024). Pan-cancer proteogenomics characterization of tumor immunity. *Cell*, *187*(5), 1255–1277.e27.
- Qin, Y., Liu, H., Huang, X., Huang, L., Liao, L., Li, J., Zhang, L., Li, W., & Yang, J. (2022). GIMAP7 as a Potential Predictive Marker for Pan-Cancer Prognosis and Immunotherapy Efficacy. *J Inflamm Res*, *15*, 1047–1061.
- Rappaport, N., Twik, M., Plaschkes, I., Nudel, R., Iny Stein, T., Levitt, J., Gershoni, M., Morrey, C., Safran, M., & Lancet, D. (2017). MalaCards: an amalgamated human disease compendium with diverse clinical and genetic annotation and structured search. *Nucleic Acids Res*, *45*(D1), D877–D887.
- Rozanova, S., Barkovits, K., Nikolov, M., Schmidt, C., Urlaub, H., & Marcus, K. (2021). Quantitative mass spectrometry-based proteomics: An overview. *Methods Mol Biol*, *2228*, 85–116.
- Ruffin, A., Cillo, A., Tabib, T., et al. (2021). B cell signatures and tertiary lymphoid structures contribute to outcome in head and neck squamous cell carcinomas. *Nat Commun*, *12*(1), 3349.
- Seal, R., Braschi, B., Gray, K., Jones, T., Tweedie, S., Haim-Vilmovsky, L., & Bruford, E. (2023). Gene-names.org: the HGNC resources in 2023. *Nucleic Acids Res*, *51*(D1), D1003–D1009.
- Short, M., Fohner, A., Skjellegrind, H., Beiser, A., Gonzales, M., Satizabal, C., et al. (2023). Proteome network analysis identifies potential biomarkers for brain aging. *J Alzheimers Dis*, *96*(4), 1767–1780.
- Shutta, K., De Vito, R., Scholtens, D., & Balasubramanian, R. (2022). Gaussian graphical models with applications to omics analyses. *Statistics in Medicine*, *41*, 5150–5187.
- Stelzer, G., Rosen, N., Plaschkes, I., Zimmerman, S., Twik, M., Fishilevich, S., et al. (2016). The GeneCards suite: from gene data mining to disease genome sequence analyses. *Curr Protoc Bioinform*, *54*, 1.30.1–1.30.33.
- Tibshirani, R. (1996). Regression shrinkage and selection via the lasso. *Journal of the Royal Statistical Society: Series B*, *58*, 267–288.
- Tutz, G., & Ulbricht, J. (2009). Penalized regression with correlation-based penalty. *Statistics and Computing*, *19*, 239–253.
- Vella, D., Zoppis, I., Mauri, G., Mauri, P., & Di Silvestre, D. (2017). From protein-protein interactions to protein co-expression networks: A new perspective to evaluate large-scale proteomic data. *EURASIP J Bioinform Syst Biol*, *2017*(1), 6.
- Villanueva, E., Smith, T., Pizzinga, M., Elzek, M., Queiroz, R. M., Harvey, R. F., Breckels, L. M., Crook, O. M., Monti, M., Dezi, V., et al. (2024). System-wide analysis of rna and protein subcellular localization dynamics. *Nature Methods*, *21*(1), 60–71.
- Wang, Y., Li, L., Li, J., & Huang, H. (2021). Network modeling in biology: Statistical methods for gene and brain networks. *Stat Sci*, *36*, 89–108.
- Weir, C., & Jan, A. (2023). *Bmi classification percentile and cut off points*. StatPearls [Internet].

- Wisniewski, J., Dus-Szachniewicz, K., Ostasiewicz, P., Ziolkowski, P., Rakus, D., & Mann, M. (2015). Absolute proteome analysis of colorectal mucosa, adenoma, and cancer reveals drastic changes in fatty acid metabolism and plasma membrane transporters. *J Proteome Res*, *14*(9), 4005–4018.
- Xu, X., Khunsriraksakul, C., Eales, J. M., Rubin, S., Scannali, D., Saluja, S., Talavera, D., Markus, H., Wang, L., Drzal, M., et al. (2024). Genetic imputation of kidney transcriptome, proteome and multi-omics illuminates new blood pressure and hypertension targets. *Nature Communications*, *15*(1), 2359.
- Yang, W., Moon, H., Kim, H., Choi, E., Yu, M., Noh, D., & Lee, C. (2012). Proteomic approach reveals fkbp4 and s100a9 as potential prediction markers of therapeutic response to neoadjuvant chemotherapy in patients with breast cancer. *J Proteome Res*, *11*(2), 1078–1088.
- Yoshihara, K., Shahmoradgoli, M., Martinez, E., et al. (2013). Inferring tumour purity and stromal and immune cell admixture from expression data. *Nat Commun.*, *4*, 2612.
- Yuan, M., & Lin, Y. (2007). On the non-negative garrotte estimator. *Journal of the Royal Statistical Society: Series B*, *69*(2), 143–161.
- Zhang, C., Zheng, J., Lin, Z., et al. (2020). Profiles of immune cell infiltration and immune-related genes in the tumor microenvironment of osteosarcoma. *Aging (Albany NY)*, *12*(4), 3486–3501.
- Zou, H. (2006). The adaptive lasso and its oracle properties. *Journal of the American Statistical Association*, *101*(476), 1418–1429.
- Zou, H., & Hastie, T. (2005). Regularization and variable selection via the elastic net. *Journal of the Royal Statistical Society: Series B*, *67*(2), 301–320.
- Zou, H., & Zhang, H. (2009). On the adaptive elastic-net with a diverging number of parameters. *Annals of Statistics*, *37*(4), 1733–1751.

## Appendix

### Proof of Theorem 1

We first derive the joint asymptotic normality part. For any  $\boldsymbol{\alpha} \in \mathbb{R}^t$ ,  $\boldsymbol{\beta} \in \mathbb{R}^q$ , denote  $\boldsymbol{\theta} = (\boldsymbol{\alpha}^\top, \boldsymbol{\beta}^\top)^\top$ ,  $\hat{\boldsymbol{\theta}}_n = (\hat{\boldsymbol{\alpha}}_n^\top, \hat{\boldsymbol{\beta}}_n^\top)^\top$ , and  $\boldsymbol{\theta}_0 = (\boldsymbol{\alpha}_0^\top, \boldsymbol{\beta}_0^\top)^\top$ . Define  $\mathbf{u} = \sqrt{n}(\boldsymbol{\theta} - \boldsymbol{\theta}_0)$  and  $\hat{\mathbf{u}}_n = \sqrt{n}(\hat{\boldsymbol{\theta}}_n - \boldsymbol{\theta}_0)$ . Then the objective function  $L_n(\boldsymbol{\alpha}, \boldsymbol{\beta})$  can be re-written as

$$L_n(\mathbf{u}) = \|Y - (\mathbf{U}, \mathbf{N})^\top \left( \boldsymbol{\theta}_0 + \frac{\mathbf{u}}{\sqrt{n}} \right)\|_2^2 + \lambda_n \sum_{s=t+1}^{t+q} \hat{w}_s \left| \theta_{0s} + \frac{u_s}{\sqrt{n}} \right|.$$

It is then easy to verify that  $\hat{\mathbf{u}}_n = \arg \min_{\mathbf{u}} L_n(\mathbf{u})$ . Note that  $L_n(\mathbf{u}) - L_n(\mathbf{0}) = V_n(\mathbf{u})$  where

$$\begin{aligned} V_n(\mathbf{u}) = \mathbf{u}^\top n^{-1} \begin{pmatrix} \mathbf{U}^\top \mathbf{U} & \mathbf{U}^\top \mathbf{N} \\ \mathbf{N}^\top \mathbf{U} & \mathbf{N}^\top \mathbf{N} \end{pmatrix} \mathbf{u} - 2 \frac{\boldsymbol{\epsilon}^\top (\mathbf{U}, \mathbf{N})}{\sqrt{n}} \mathbf{u} \\ + \frac{\lambda_n}{\sqrt{n}} \sum_{s=t+1}^{t+q} \hat{w}_s \sqrt{n} \left( \left| \theta_{0s} + \frac{u_s}{\sqrt{n}} \right| - |\theta_{0s}| \right). \end{aligned}$$

The first term in the above display converges to  $\mathbf{u}^\top \mathbf{C} \mathbf{u}$  for every  $\mathbf{u}$ . For the second term, by the Central Limit Theorem, we obtain  $\boldsymbol{\epsilon}^\top (\mathbf{U}, \mathbf{N}) / \sqrt{n} \rightarrow_d \mathbf{W} = N(0, \sigma^2 \mathbf{C})$ . The limiting behavior of the last term

depends on whether  $\theta_{0s}$  is active or not for  $s = t + 1, \dots, t + q$ , which is equivalent to as whether  $\beta_{0j}$  is active or not for  $j = 1, \dots, q$ . Note that if  $\beta_{0j} \neq 0$ , then  $\tilde{\beta}_{nj} \rightarrow_p \beta_{0j}$  and  $\hat{w}_j = |\tilde{\beta}_{nj}|^{-\nu} \rightarrow_p |\beta_{0j}|^{-\nu}$  by the Continuous Mapping Theorem. Also,  $\sqrt{n} \left( \left| \beta_{0j} + \frac{u_j}{\sqrt{n}} \right| - |\beta_{0j}| \right) = u_j \text{sgn}(\beta_{0j})$ . Hence, by Slutsky's Theorem,  $\frac{\lambda_n}{\sqrt{n}} \hat{w}_j \sqrt{n} \left( \left| \beta_{0j} + \frac{u_j}{\sqrt{n}} \right| - |\beta_{0j}| \right) \rightarrow_p 0$ . If  $\beta_{0j} = 0$ , then  $\sqrt{n} \left( \left| \beta_{0j} + \frac{u_j}{\sqrt{n}} \right| - |\beta_{0j}| \right) = |u_j|$  and  $\frac{\lambda_n}{\sqrt{n}} \hat{w}_j = \frac{\lambda_n}{\sqrt{n}} n^{\nu/2} (|\sqrt{n} \tilde{\beta}_{nj}|)^{-\nu} \rightarrow \infty$  since  $\sqrt{n} \tilde{\beta}_{nj} = O_p(1)$ . Therefore, the last term converges in probability to 0 if  $\theta_{0s} \neq 0$ , and it converges to  $\infty$  if  $\theta_{0s} = 0$ . Now let  $\mathcal{S} = \{1, 2, \dots, t\} \cup \{s : \theta_{0s} \neq 0, s = t + 1, \dots, t + q\}$ . Then by Slutsky's Theorem, we get  $V_n(\mathbf{u}) \rightarrow_d V(\mathbf{u})$  for every  $\mathbf{u}$ , where

$$V(\mathbf{u}) = \begin{cases} \mathbf{u}_{\mathcal{S}}^{\top} \mathbf{C}_{\mathcal{S}} \mathbf{u}_{\mathcal{S}} - 2\mathbf{u}_{\mathcal{S}}^{\top} \mathbf{W}_{\mathcal{S}} & \text{if } u_s = 0 \text{ for } s \notin \mathcal{S} \\ \infty & \text{otherwise} \end{cases}$$

Note that  $V(\mathbf{u})$  is convex and the minimum of  $V(\mathbf{u})$  is uniquely achieved at  $(\mathbf{C}_{\mathcal{S}}^{-1} \mathbf{W}_{\mathcal{S}}, \mathbf{0})^{\top}$  where  $\mathbf{C}_{\mathcal{S}}^{-1} \mathbf{W}_{\mathcal{S}} \in \mathbb{R}^{t+r}$  and  $\mathbf{0} \in \mathbb{R}^{q-r}$ . By the epi-convergence results of Geyer, 1994 and Knight and Fu, 2000, we have

$$\hat{\mathbf{u}}_{n\mathcal{S}} \rightarrow_d \mathbf{C}_{\mathcal{S}}^{-1} \mathbf{W}_{\mathcal{S}} \quad \text{and} \quad \hat{\mathbf{u}}_{n\mathcal{S}^c} \rightarrow_d \mathbf{0}. \quad (.1)$$

Therefore,  $\hat{\mathbf{u}}_{n\mathcal{S}} = \sqrt{n} \left( \frac{\hat{\boldsymbol{\alpha}}_n - \boldsymbol{\alpha}_0}{\hat{\boldsymbol{\beta}}_{n\mathcal{J}} - \boldsymbol{\beta}_{0\mathcal{J}}} \right) \rightarrow_d \mathbf{C}_{\mathcal{S}}^{-1} \mathbf{W}_{\mathcal{S}} = N(\mathbf{0}, \sigma^2 \mathbf{C}_{\mathcal{S}}^{-1})$ , where  $\mathbf{C}_{\mathcal{S}} \in \mathbb{R}^{(t+r) \times (t+r)}$  is the top-left block matrix (i.e., sub-matrix) of  $\mathbf{C} \in \mathbb{R}^{(t+q) \times (t+q)}$ .

Now we show the consistency part. Note that the asymptotic normality results imply that  $\hat{\boldsymbol{\alpha}}_n \rightarrow_p \boldsymbol{\alpha}_0$  and  $\hat{\boldsymbol{\beta}}_{nj} \rightarrow_p \beta_{0j}$  for  $\forall j \in \mathcal{J}$ , and hence  $P(j \in \hat{\mathcal{J}}_n) \rightarrow 1$ . Then it suffices to show that  $\forall j' \notin \mathcal{J}$ ,  $P(j' \in \hat{\mathcal{J}}_n) \rightarrow 0$ . When  $j' \in \hat{\mathcal{J}}_n$ , we observe that  $2N_{j'}^{\top} (Y - \mathbf{U} \hat{\boldsymbol{\alpha}}_n - \mathbf{N} \hat{\boldsymbol{\beta}}_n) = \lambda_n \hat{w}_{j'} \text{sgn}(\hat{\beta}_{nj'})$  by the Karush-Kuhn-Tucker (KKT) conditions. Note that  $\lambda_n \hat{w}_{j'} \text{sgn}(\hat{\beta}_{nj'}) / \sqrt{n} = \frac{\lambda_n}{\sqrt{n}} n^{\nu/2} \frac{1}{|\sqrt{n} \hat{\beta}_{nj'}|^{\nu}} \text{sgn}(\hat{\beta}_{nj'}) \rightarrow_p \infty$ , whereas

$$\begin{aligned} 2N_{j'}^{\top} (Y - \mathbf{U} \hat{\boldsymbol{\alpha}}_n - \mathbf{N} \hat{\boldsymbol{\beta}}_n) / \sqrt{n} &= 2N_{j'}^{\top} \mathbf{U} \sqrt{n} (\boldsymbol{\alpha}_0 - \hat{\boldsymbol{\alpha}}_n) / n \\ &\quad + 2N_{j'}^{\top} \mathbf{N} \sqrt{n} (\boldsymbol{\beta}_0 - \hat{\boldsymbol{\beta}}_n) / n + 2N_{j'}^{\top} \boldsymbol{\epsilon} / \sqrt{n}. \end{aligned}$$

By (.1) and Slutsky's Theorem, we know that  $2N_{j'}^{\top} \mathbf{U} \sqrt{n} (\boldsymbol{\alpha}_0 - \hat{\boldsymbol{\alpha}}_n) / n$  and  $2N_{j'}^{\top} \mathbf{N} \sqrt{n} (\boldsymbol{\beta}_0 - \hat{\boldsymbol{\beta}}_n) / n$  converges in distribution to some normal distribution and  $2N_{j'}^{\top} \boldsymbol{\epsilon} / \sqrt{n} \rightarrow_d N(\mathbf{0}, 4\|N_{j'}\|_2^2 \sigma^2)$ . Hence,  $P(j' \in \hat{\mathcal{J}}_n) \leq P\left(2N_{j'}^{\top} (Y - \mathbf{U} \hat{\boldsymbol{\alpha}}_n - \mathbf{N} \hat{\boldsymbol{\beta}}_n) = \lambda_n \hat{w}_{j'} \text{sgn}(\hat{\beta}_{nj'})\right) \rightarrow 0$ . This proves the consistency part.